Synthesis and characterization of the $La_{1-x}Sr_xFeO_{3-\delta}$ system and the fluorinated phases $La_{1-x}Sr_xFeO_{3-x}F_x$

Oliver Clemens [*], Melanie Kuhn [1], Robert Haberkorn

Anorganische Festkörperchemie, Universität des Saarlandes, Dudweiler, Am Markt, Zeile 3, 66125 Saarbrücken, Germany

A B S T R A C T

The oxyfluorides $La_{1-x}Sr_xFeO_{3-x}F_x$ have been prepared by fluorination of the precursor oxides $La_{1-x}Sr_xFeO_{3-\delta}$ via a low temperature route using poly(vinylidene fluoride) (PVDF). The structures of the oxides and oxyfluorides were investigated in detail by the Rietveld analysis of powder diffraction data. The oxyfluorides crystallize in the space group *Pnma* for $0 < x \leq 0.9$ (SrFeO₂F itself is cubic, space group *Pm-3m*) and show a sort of two-step structural distortion for decreasing x. Furthermore, a structural comparison of the oxyfluorides with the oxides is given, revealing an increase of the volume per $La_{1-x}Sr_xFeX_3$ unit during fluorination, of which the magnitude highly depends on the value of x.

© 2011 Elsevier Inc. All rights reserved.

1. Introduction

Perovskite ($A^{[12]}B^{[6]}X_3$) type $La_{1-x}Sr_xFeO_{3-\delta}$ oxides find wide applications as solid oxide fuel cell cathodes [1], battery materials [2], oxygen separation membranes [3], catalysts for the partial oxidation of methane [4], in membrane reactors for hydrogen production [5], as gas sensors [6], etc. The solid solution $La_{1-x}Sr_xFeO_{3-\delta}$ has a high stability even under reducing atmospheres [7]. Its structural tolerance for large oxygen nonstoichiometry and the mixed valence state of the B-site transition metal result in mixed electronic and ionic conductivity [1,7–9]. Moreover, $La_{1-x}Sr_xFeO_{3-\delta}$ shows a semi-conducting behavior where the electrical conduction is p-type at higher oxygen partial pressures with electron hopping between Fe^{3+} and Fe^{4+} ions and n-type with electron exchange between Fe^{3+} and Fe^{2+} ions under reducing atmospheres [8].

$La_{1-x}Sr_xFeO_{3-\delta}$ ($\delta \approx 0$) undergoes phase changes from orthorhombic through rhombohedral to cubic with increasing strontium dopant content [10–12]. For $x < 0.6$, such oxygen stoichiometric samples can even be prepared by quenching from 1300 °C in air, and annealing at lower temperatures in air favors the uptake of oxygen for Sr richer samples (higher values of x) [11]. For compositions near a phase transition, mixtures of multiple phases were detected [11]. Based on the Mössbauer analysis [11,12], the structural changes are attributed to varying oxidation states of iron leading to changes in ionic size and ordering of oxygen. Changes in the magnetic properties coincide with the phase transitions.

Interest in fluorination of oxide materials mainly grew after the discovery of superconductivity in $Sr_2CuO_2F_{2+\delta}$ [13–15]. For the synthesis of such mixed oxyfluorides, which are often metastable and decompose at higher temperatures [16], low temperature fluorination often needs to be applied. Due to the high stability of the alkaline earth fluorides and LnOF these are the decomposition products [16]. Therefore, many oxyfluorides are only kinetically stabilized products and high temperature synthesis methods are usually not successful for their preparation (a known exception to this rule of thumb is BaFeO₂F, which can also be prepared under high pressure at 1000 °C [17]). Common fluorination agents are CuF₂, ZnF₂, NH₄F, F₂ and XeF₂ [13–15,18,19], which differ in their reaction characteristics [16]. Another promising fluorination agent is poly(vinylidene fluoride) (PVDF), which could be used successfully for the synthesis of Ca₂CuO₂F₂ [16], Sr₂CuO₂F₂ [16], the perovskites SrFeO₂F [20], BaFeO₂F [21], SrₓBa₁₋ₓFeO₂F [22,23], $SrFe_{1-x}Sn_xO_{2+x}F_{1-x}$ (x=0.31, 0.54) [24] and $La_{1-x}Sr_xFe_{1-y}Co_yFeO_{3-x}F_x$ (x=1, 0.9, y=1, 0.5) [25].

Fluorination may also have an impact on magnetic ordering and conductivity: In two recent studies, Berry et al. showed that the cubic perovskites SrFeO₂F [26] and BaFeO₂F [27], although

structurally very similar, are substantially different with respect to their magnetic properties. Furthermore, Sturza et al. [28] showed that the incorporation of F^- into (Ba/Sr)Fe based hexagonal perovskites yields extended defect structures, which show reversible incorporation/removal of oxygen and ionic conductivity at low temperatures.

In this paper, we report the synthesis and structural characterization of the system $La_{1-x}Sr_xFeO_{3-x}F_x$ $(0 < x \le 1)$ and compare these fluorinated phases with their precursor oxides $La_{1-x}Sr_xFeO_{3-\delta}$.

2. Experimental details

2.1. Sample synthesis

Compounds of the composition $La_{1-x}Sr_xFeO_{3-\delta}$ with a strontium content of $x=0–1$ were prepared by a solid state reaction. High-purity La_2O_3, $SrCO_3$ and Fe_2O_3 powders (Merck KGaA, Darmstadt, Germany) were mixed in the appropriate stoichiometric ratio and were thoroughly ground in n-pentane. The La_2O_3 powder was first calcined at 1100 °C for 12 h to remove any water content. The ground powders were twice heat treated in air at 1250 °C for 30 h with intermediate grinding and slowly cooled down to room temperature. Nearly stoichiometric oxygen content can be assumed for samples with $x < 0.6$ for such a cooling procedure, and deficiency δ for higher x is lower than ~ 0.125 or nearly equal to that value $(x=1)$ [7,11,12].

For fluorination, the $La_{1-x}Sr_xFeO_3$ compounds were mixed with a 10% excess of poly(vinylidene fluoride) PVDF (Sigma-Aldrich Chemie GmbH, Steinheim, Germany). After thoroughly grinding, the mixtures were heated in air at 673 °C for 15 h.

Decomposition of oxyfluoride samples was performed at 950 °C in dry air for 2 h followed by slow cooling to room temperature.

2.2. Diffraction experiments

XRD measurements of the oxides, oxyfluorides and decomposed samples were performed using a Panalytical X'Pert Pro diffractometer with focusing Bragg–Brentano geometry and a fine focus X-ray tube with Cu anode in a 2θ-range from 10° to 110° at a total scan time of 1 h. No primary beam monochromator was attached. A fast PIXcel detector and a variable divergence slit were used. The whole 2θ-range was used for Rietveld analysis by the program TOPAS 4.2 (Bruker AXS, Karlsruhe, Germany) [29]. The instrumental intensity distribution was determined empirically based on the fundamental parameters set for a reference scan of LaB_6 [30]. Positional, microstructural and lattice parameters were refined during the Rietveld

analysis. The displacement parameters of all atoms of all phases were constraint to an overall B-value to minimize errors of phase quantification. Based on our experience, the standard deviations for the lattice parameters given in this article are the ones calculated by the Rietveld procedure multiplied by 4.

3. Results and discussion

3.1. $La_{1-x}Sr_xFeO_{3-\delta}$

The previously reported phase transitions [11,12] with increasing strontium content in $La_{1-x}Sr_xFeO_{3-\delta}$ were confirmed in this study (see Table 1). For $x=0$ and 0.1, the XRD patterns were refined using an orthorhombic phase in the space group $Pnma$ (isostructural to $GdFeO_3$ [31]). A mixture of orthorhombic and rhombohedral phase (space group $R-3c$) was observed for compounds with $0.2 \le x \le 0.4$ where the rhombohedral fraction increased with x and became the only phase for $x=0.5$ and 0.6. A phase transition to cubic ($Pm-3m$) then occurred followed by a transition to the tetragonal modification ($I4/mmm$) for $x=0.9$ and 1, which is caused by the ordering of oxygen vacancies $(\delta \approx 0.125)$ [32]. For lower values of x, such ordering cannot be maintained due to the increasing oxygen content [7,11,12]. Table 1 summarizes the lattice parameters and refined weight fractions of the respective phases. The lattice parameters are in good agreement with [11,12]. Example XRD patterns are shown in Fig. 1.
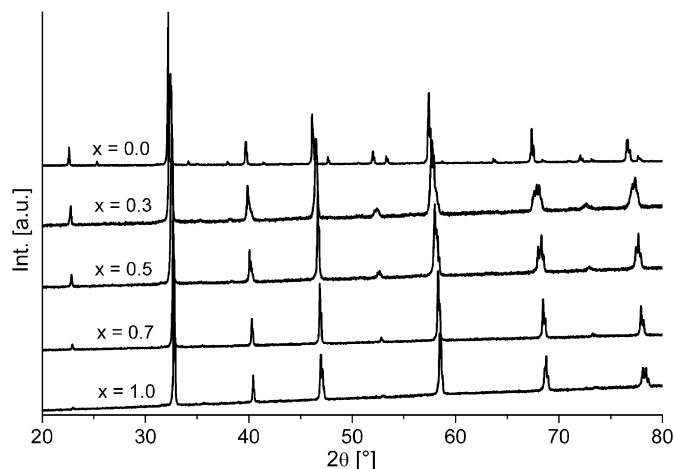

Fig. 1. XRD patterns of $La_{1-x}Sr_xFeO_{3-\delta}$ (with $x=0$, 0.3, 0.5, 0.7 and 1) heated in air.

Table 1
Refined lattice parameters and pseudo cubic lattice parameter $a_{f.u.}$ for samples of composition $La_{1-x}Sr_xFeO_{3-\delta}$.

x in $La_{1-x}Sr_xFeO_{3-\delta}$	Space group/weight fraction (%)	a (Å)	b (Å)	c (Å)	$a_{f.u.}$ (Å)
0.0	Pnma	5.5666 (1)	7.8551 (2)	5.5553 (1)	3.9306
0.1	Pnma	5.546 (1)	7.844 (3)	5.554 (2)	3.9235
0.2	Pnma (72)	5.5183 (4)	7.8117 (8)	5.5510 (8)	3.9110
	R-3c (28)	5.5526 (8)		13.578 (4)	3.9241
0.3	Pnma (50)	5.5082 (4)	7.7942 (8)	5.5501 (8)	3.9055
	R-3c (50)	5.5403 (4)		13.427 (2)	3.9037
0.4	Pnma (11)	5.495 (2)	7.795 (3)	5.521 (2)	3.8956
	R-3c (89)	5.5276 (2)		13.4211 (8)	3.8972
0.5	R-3c (100)	5.5105 (2)		13.4164 (8)	3.8887
0.6	R-3c (100)	5.4952 (2)		13.4136 (4)	3.8812
0.7	Pm-3m (100)	3.87246 (8)			3.8725
0.8	Pm-3m (100)	3.86782 (8)			3.8678
0.9	I4/mmm (100)	10.9418 (4)		7.7161 (4)	3.8650
1.0	I4/mmm (100)	10.938 (1)		7.7024 (8)	3.8618

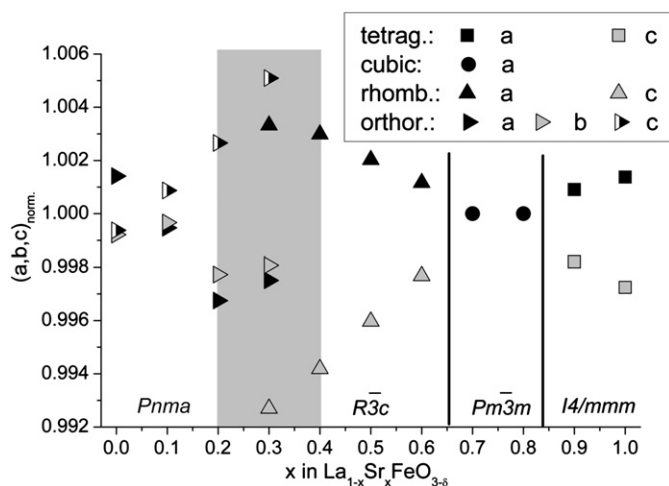**Fig. 2.** Dependence of the metric distortion from cubic symmetry $(a,b,c)_{norm}$ on x for $La_{1-x}Sr_xFeO_{3-\delta}$. The range of x where the rhombohedral and orthorhombic phases are found simultaneously is marked by a gray box.

Fig. 2 shows the degree of metric distortion from cubic symmetry, which we define as

$$(a,b,c)_{norm} = \frac{(a,b,c)}{k\sqrt[3]{V_{f.u.}}}$$

with $k=1$ for a_{cubic}, $k=\sqrt{2}$ for $a_{orthor.}$, $c_{orthor.}$, $a_{rhomb.}$, $k=2$ for $b_{orthor.}$, $c_{tetr.}$, $k=2\sqrt{2}$ for $a_{tetr.}$ and $k=2\sqrt{3}$ for $c_{rhomb.}$ to normalize the lattice parameters to a pseudo-cubic size taking into account the orientation of the lower symmetry cells with respect to the cubic one. $V_{f.u.}$ can be considered as the pseudo-cubic cell volume, calculated as the volume per $La_{1-x}Sr_xFeO_{3-\delta}$ formula unit (resp. $La_{1-x}Sr_xFeO_{3-x}F_x$ in Section 3.2). Then $\sqrt[3]{V_{f.u.}}$ may be taken as a pseudo-cubic lattice parameter $a_{f.u.}$. If $(a,b,c)_{norm}$ is close to 1, the respective lattice parameter deviates only little from an ideal cubic one. For $x=0.2$ and $x=0.4$, $(a,b,c)_{norm}$ is shown for the main phase only. Small distortions are observed for the lanthanum-rich orthorhombic compounds. The magnitude of the distortion increases with increase in strontium content reaching a maximum for $x=0.3$. The distortion then decreases when further adding strontium and disappears completely for $x=0.7$ and 0.8 showing a cubic structure. For $x=0.9$ and $SrFeO_{3-\delta}$ itself, the distortion again increases, resulting in a fish-shaped plot as given in Fig. 2.

3.2. $La_{1-x}Sr_xFeO_{3-x}F_x$ and comparison with the precursor phases $La_{1-x}Sr_xFeO_{3-\delta}$

All oxyfluorides were obtained as fine powders of brown color, where the color can be considered as a first indication that only trivalent iron is present. In contrast to $BaFeO_2F$ and $SrFeO_2F$, the degree of fluorination x depends on the lanthanum content of the sample and may be assumed to show a maximal fluorination according to the formula $La_{1-x}Sr_xFeO_{3-x}F_x$. La richer samples can therefore be fluorinated to a much lower extent than Sr rich samples, since they contain more oxygen per se than Sr richer ones. Higher fluoride contents $La_{1-x}Sr_xFeO_{3-x-\sigma}F_{x+\sigma}$ would cause the formation of divalent iron and this has not been observed for fluorinations using PVDF, even when heating was performed under N_2 and the polymer itself was used in a much higher excess [25]. Since the oxyfluorides are not thermodynamically stable due to the high stability of SrF_2, the fluoride content can be determined by decomposition of the samples at higher temperatures and analysis and quantification of the decomposition products by the Rietveld method, which was an easy way to confirm the composition of $SrFeO_2F$ [22]. This method was applied to the phase mixtures yielded by decomposition

assuming as products a cubic SrF_2 phase (confirmed by a comparison to the lattice parameter given by literature [33]) and a perovskite-type phase $La_{1-d}Sr_dFeO_3$, where d was refined. The refined weight fractions of all phases then allow calculation of an approximate formula of the composition of the sample. For $x=0.8$ and 0.9, the refined compositions of $La_{0.20}Sr_{0.64}FeO_{2.17}F_{0.76}$ and $La_{0.13}Sr_{0.82}FeO_{2.24}F_{0.88}$ approximately confirm the assumed formulas of the fluorination products, since the Fe/F ratio is sufficiently fulfilled. For lower values of x (La richer and F poorer samples), such a quantitative phase analysis becomes more difficult, because for these samples F^- seems to remain partly present in the perovskite phase after decomposition. This is confirmed by comparison of the cell volumes per $La_{1-x}Sr_xFeX_3$ unit, which are very indicative (see later in this section). Such increased stability towards decomposition was also observed for hexagonal fluorine containing perovskites $15R-BaFeF_cO_{3-\delta}$ $(0.15 \leq c \leq 0.35)$ and $6H-Ba_{0.8}Sr_{0.2}FeF_c$ $O_{3-\delta}$ $(0.15 \leq c \leq 0.25)$ [28,34]. Nevertheless, SrF_2 is always found as a decomposition product in our case.

$SrFeO_2F$ is obtained as a cubic perovskite (space group Pm-$3m$), which is in agreement with previous findings [20–22]. All other oxyfluorides $La_{1-x}Sr_xFeO_{3-x}F_x$ $(0 < x \leq 0.9)$ crystallize in the orthorhombic space group $Pnma$ and are isotypic to $LaFeO_3$ (Fig. 3 and Table 2). It is very remarkable that single phase oxyfluorides are found even when the starting mixture $La_{1-x}Sr_xFeO_{3-\delta}$ was composed of a biphasic mixture of a rhombohedral and an orthorhombic phase $(0.2 \leq x \leq 0.4)$. This is surprising, since the low fluorination temperature of 400 °C probably does not allow for a redistribution of the A site cations [22].

The refined average distances Fe–O/F in the 6 or 5-fold coordination (see Section 3.1) for the oxides and oxyfluorides are given in Table 3. The Fe–O distances for the oxides are generally smaller compared to the oxyfluorides, which is explained by an increasing Fe^{4+}/Fe^{3+} ratio for increasing x in $La_{1-x}Sr_xFeO_{3-\delta}$. Larger Fe–O distances for the oxide samples with $x=0.9$–1.0 compared to the oxide samples with slightly lower x (0.7–0.8) indicate furthermore the formation of oxygen vacancies in the former samples, which is accompanied by the formation of Fe^{3+} [32]. For the oxyfluorides, the refined average Fe–O/F distances indicate the formation of Fe^{3+} from comparison with calculated $Fe^{3+}-O_{3-x}F_x$ distances from the Shannon radii [35]. As can be seen in Table 3, the calculated distances are about 0.04 Å higher than the refined distances; nevertheless, this is also the case for $SrFeO_2F$ and $LaFeO_3$, which have been shown to contain trivalent iron only [20,22,26].

Keeping in mind that the metric distortion for $x=0.9$ and 1 in $La_{1-x}Sr_xFeO_{3-\delta}$ is caused by a high degree and ordering of vacancies

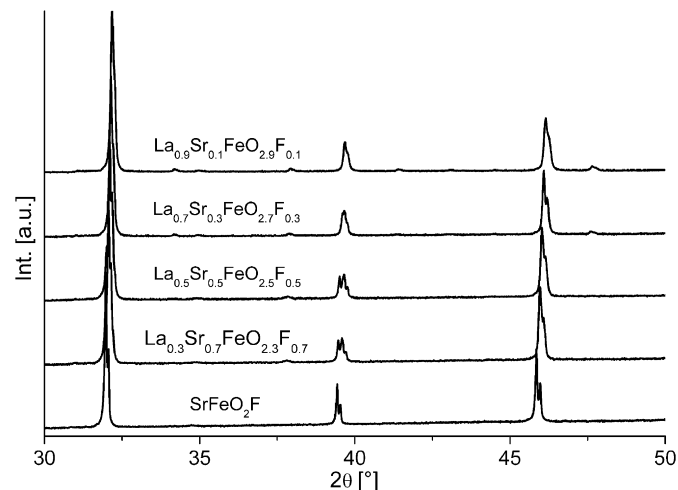**Fig. 3.** XRD patterns of the samples with composition $La_{1-x}Sr_xFeO_{3-x}F_x$.

Table 2
Refined lattice parameters and pseudo-cubic lattice parameter $a_{f.u.}$ for fluorination products of composition $La_{1-x}Sr_xFeO_{3-x}F_x$ and $LaFeO_3$.

x in $La_{1-x}Sr_xFeO_{3-x}F_x$	Space group	a (Å)	b (Å)	c (Å)	$a_{f.u.}$ (Å)
1.0	Pm-$3m$	3.95494 (4)			3.9549
0.9	$Pnma$	5.5847 (4)	7.9105 (5)	5.5890 (4)	3.9521
0.8	$Pnma$	5.5732 (2)	7.8922 (5)	5.5962 (2)	3.9480
0.7	$Pnma$	5.5668 (2)	7.8848 (4)	5.5955 (2)	3.9451
0.6	$Pnma$	5.5609 (2)	7.8783 (3)	5.5926 (2)	3.9419
0.5	$Pnma$	5.5586 (2)	7.8746 (3)	5.5892 (2)	3.9400
0.4	$Pnma$	5.5606 (2)	7.8734 (3)	5.5801 (4)	3.9381
0.3	$Pnma$	5.5606 (3)	7.8694 (4)	5.5736 (2)	3.9359
0.2	$Pnma$	5.5605 (2)	7.8678 (4)	5.5662 (2)	3.9339
0.1	$Pnma$	5.5596 (2)	7.8587 (3)	5.5616 (3)	3.9311
0.0	$Pnma$	5.5666 (1)	7.8551 (2)	5.5553 (1)	3.9306

Table 3
Observed average Fe–O/F distances $\langle d(Fe$–$X)\rangle_{obs.}$ for samples of composition $La_{1-x}Sr_xFeO_{3-x}F_x$ and $La_{1-x}Sr_xFeO_{3-\delta}$ and comparison to theoretical Fe–O/F distances $d(Fe$–$O)_{calc.}$ calculated after [35] for 6-fold coordination.
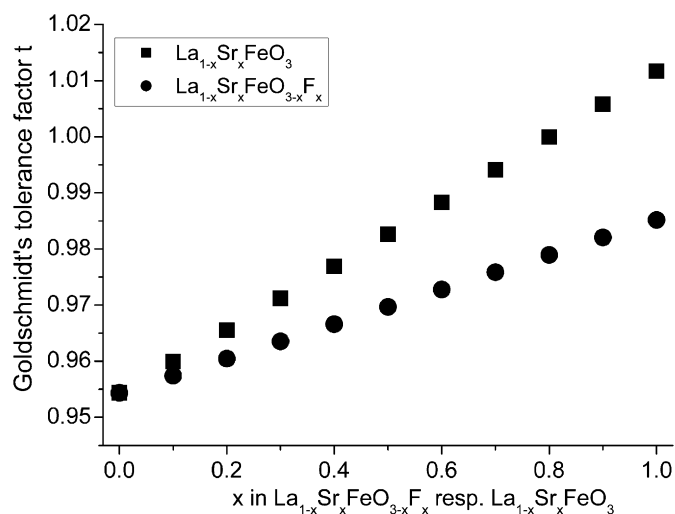
x in $La_{1-x}Sr_xFeO_{3-x}F_x$ resp. $La_{1-x}Sr_xFeO_{3-\delta}$	$La_{1-x}Sr_xFeO_{3-x}F_x$			$La_{1-x}Sr_xFeO_{3-\delta}$		
	$\langle d(Fe$-$(X))\rangle_{obs.}$ and space group		$d(Fe$-$X)_{calc.}$	$\langle d(Fe$–$X)\rangle_{obs.}$, [CN] and space group		$d(Fe$-$X)_{calc.}$
0.0			2.05	2.01 [6]	$Pnma$	2.05
0.1	2.00	$Pnma$	2.04	2.00 [6]	$Pnma$	2.04
0.2	2.00	$Pnma$	2.04	1.98 [6]	$Pnma$	2.03
0.3	2.00	$Pnma$	2.04	1.98 [6]	$Pnma$	2.03
				1.97 [6]	R-$3c$	2.03
0.4	2.00	$Pnma$	2.04	1.96 [6]	R-$3c$	2.02
0.5	1.99	$Pnma$	2.03	1.96 [6]	R-$3c$	2.02
0.6	1.99	$Pnma$	2.03	1.95 [6]	R-$3c$	2.01
0.7	1.99	$Pnma$	2.03	1.94 [6]	Pm-$3m$	2.00
0.8	1.99	$Pnma$	2.03	1.93 [6]	Pm-$3m$	2.00
0.9	1.99	$Pnma$	2.02	1.94 [6]	$I4/mmm$	1.99
				1.95 [6]		
				1.91 [5]		
1.0	1.98	Pm-$3m$	2.02	1.93 [6]	$I4/mmm$	1.99
				1.96 [6]		
				1.91 [5]		

[32,36,37] and that the oxides are cubic for $x=0.7$ and 0.8, a deviation from cubic symmetry is already found for higher Sr content in the oxyfluorides ($x \leq 0.9$). This can be explained by considering Goldschmidt's tolerance factor [38], which can be calculated for a given perovskite $A^{[12]}B^{[6]}X_3$ from the ionic radii r [35].

$$t = \frac{r_A + r_X}{\sqrt{2}(r_B + r_X)}$$

The value of t is significantly lower for the oxyfluorides with high Sr content than in the case of the oxides and approaches the t-value of $LaFeO_3$ for La richer compositions (Fig. 4). Since deviations from cubic symmetry are observed for values of t considerably lower than 1, it becomes clear that the fluorination of $La_{1-x}Sr_xFeO_{3-\delta}$ favors the formation of non-cubic perovskites, since r_B is increased by the reduction of Fe^{4+} to Fe^{3+} [35]. Therefore, the generally higher metric distortion in the oxyfluorides compared to the oxides is explained by a higher deviation from the ideal ion size ratio for the cubic arrangement.

The volumes per formula unit of $La_{1-x}Sr_xFeO_{3-x}F_x$ and $La_{1-x}Sr_xFeO_{3-\delta}$ show increasing deviation for increasing x (Fig. 5) and the former ones generally show a larger volume than the latter ones. This can be explained by the reduction of Fe^{4+} to Fe^{3+} during exchange of O^{2-} by F^- and the larger ionic radius of trivalent iron [35] and such behavior was also observed in the case of the fluorination products of $(Sr,Ba)FeO_{3-\delta}$ [20,22,25]. It is also found that the volume increase is higher for Sr richer samples, since more Fe^{4+} is being reduced. This increase in cell volume can be considered

Fig. 4. Goldschmidt's tolerance factor for the perovskites $La_{1-x}Sr_xFeO_{3-x}F_x$ and $La_{1-x}Sr_xFeO_{3-\delta}$, calculated from radii given in [34].

as a further proof that $La_{1-x}Sr_xFeO_{3-\delta}$ could be fluorinated successfully. The volume change is even significant for La rich samples, which can be fluorinated to a much lower extent. E.g. for $x=0.2$, the increase in $V_{f.u.}$ of ~ 1 Å^3 is in the same order of magnitude than exchanging all La for Sr in the oxyfluoride samples. This means that the reduction of Fe^{4+} to Fe^{3+} during fluorination has the strongest

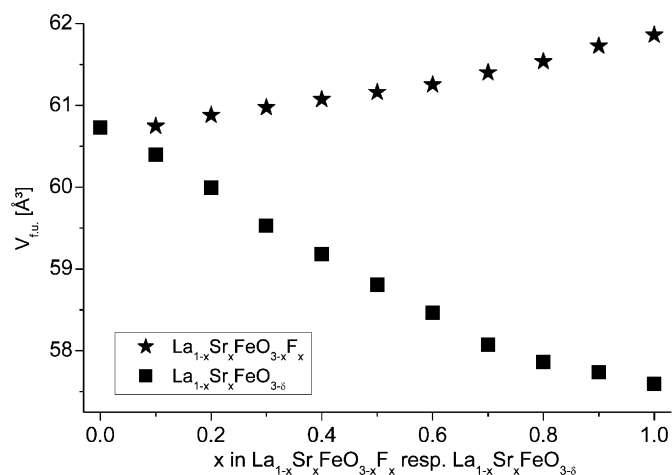**Fig. 5.** Comparison of the volume per formula unit $V_{f.u.}$ for oxide and oxyfluoride samples.

Fig. 6. Dependency of $(a,b,c)_{norm}$ on the degree of doping x in $La_{1-x}Sr_xFeO_{3-x}F_x$.

Fig. 7. Dependency of $\Delta^2(X1, X2, A)$ on the degree of doping x in $La_{1-x}Sr_xFeO_{3-x}F_x$.

Fig. 8. Effective coordination number (ECoN) of the A cation (La/Sr) for the oxyfluorides $La_{1-x}Sr_xFeO_{3-x}F_x$.

impact on the change of the cell volume. In addition, the cell volume increases for the oxyfluoride samples with increasing x, whereas it decreases for the oxides. In the oxide case, a change of the Sr/La content also means a change in the Fe^{4+}/Fe^{3+} ratio following $La_{1-x}Sr_xFe_{1-x}^{3+}Fe_x^{4+}O_3$, if a fully oxidized sample with stoichiometric oxygen content is assumed [7,12]. For the oxides, the volume decrease with higher Sr content is dominated by a higher content of Fe^{4+} (which is smaller than Fe^{3+} [35]), although Sr^{2+} itself is larger than La^{3+}. For the oxyfluorides, which contain Fe^{3+} only [20,22,25], the dependency of the cell volume on x is mainly influenced by the change of the radius of the A site cation. Since the fluorination reaction was performed in air at 400 °C followed by slow cooling, a reduction of Fe^{4+} by pure oxygen loss (which would also cause an increase of cell volume) can be ruled out, since these reaction conditions would rather favor the uptake of oxygen in the absence of a fluorination agent [11].

Furthermore, the volume change as a function of x for the oxides and oxyfluorides (Fig. 5) deviates from a straight line according to Vegard's rule, which should be expected if the volume only depended on the change of ionic radii of La/Sr (1.36–1.44 Å) [35] and O/F (1.40–1.33 Å) [35]. For the oxides, the kink between 0.7 and 0.8 can probably be explained by reaching nearly stoichiometric oxygen content for $x \leq 0.8$ [7,11,12]. For the oxyfluorides, the kink at 0.5–0.6 can be explained by considering the degree of distortion from cubic symmetry $(a,b,c)_{norm}$ (see Section 3.1). Fig. 6 shows the dependency of $(a,b,c)_{norm}$ on x for $La_{1-x}Sr_xFeO_{3-x}F_x$. Going from high (Sr rich) to low values of x, the degree of lattice parameter distortion is biggest for a and c for $x=0.5$–0.6 and decreases again for La richer samples. In contrast to a and c, the b axis deviates from the cubic symmetry to a much lower extent. The directions of distortion (<1 or >1) of a and c are usually opposed and for $x=0$, the directions are switched compared to $0.1 \leq x \leq 0.8$. Therefore, the plot of $(a,b,c)_{norm}$ vs. x (Fig. 6) again resembles a simple sketch of a "fish".

Understanding of this unusual doping behavior of the lattice parameters (the "fish") requires a deeper look into the structure. For the orthorhombic symmetry (prototype GdFeO₃ [31]), Fe^{3+} is located on the special position 0, 0, 0 ($4a$). All other ion positions ($X1$, $X2$ ($4c$, $8d$) both O/F), A ($4c$, La/Sr) allow for relaxation from their ideal position for cubic symmetry. An average deviation square from the ideal cubic position Δ can be calculated for $X1$, $X2$ and A as

$$\Delta^2(X1,X2,A) = \sqrt{2}(x-x_{ideal})^2 + 2(y-y_{ideal})^2 + \sqrt{2}(z-z_{ideal})^2 \text{ with}$$

x,y,z being the refined positional parameters and $(x,y,z)_{ideal}$ being the ideal positional parameters yielded by transformation of the
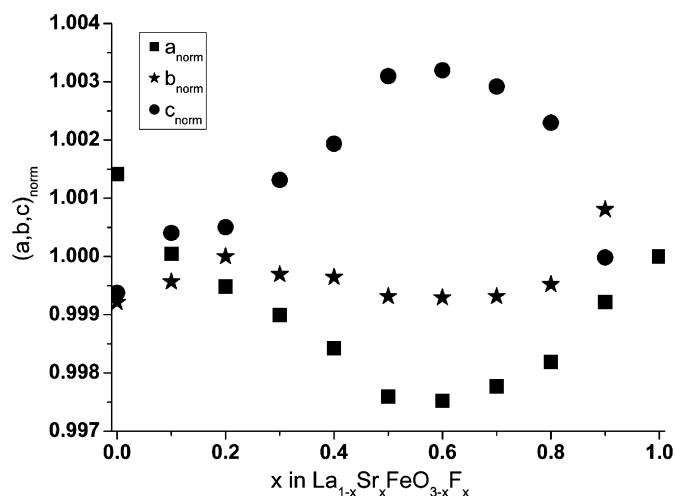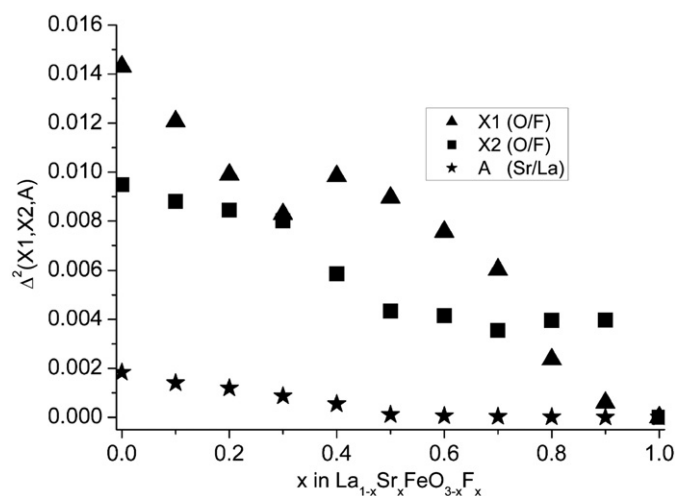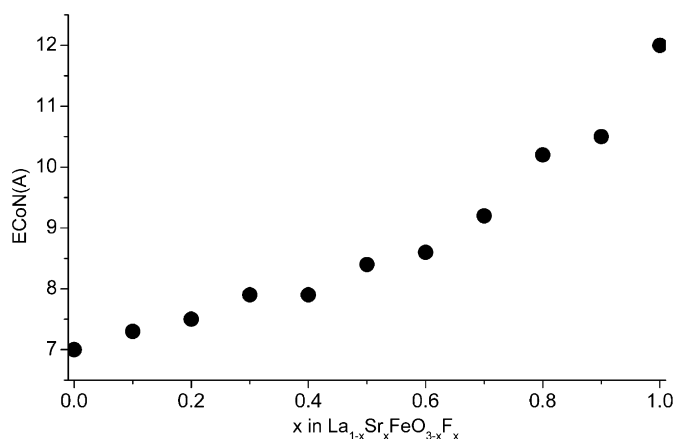
cubic perovskite into the orthorhombic setting and where the factors 2 and $\sqrt{2}$ take into account the orientation of the lower symmetry cells with respect to the cubic one. Fig. 7 shows Δ^2 as a function of x for each ion. $X1$ is shifting nearly continuously away from the ideal position with increasing La content (decreasing x),
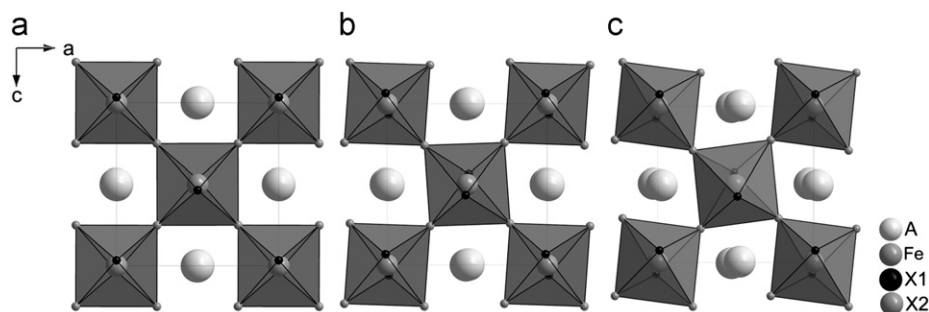
Fig. 9. Crystal structures of $La_{1-x}Sr_xFeO_{3-x}F_x$ for $x=0.8$ (a), 0.5 (b) and 0.1 (c).

which causes a first reduction of the effective coordination number (ECoN [39]) of the A cation (see Fig. 8). The ECoN was calculated assuming an average ionic radius of O/F in 6-fold coordination and random distribution of these anions on the anion sites. $X2$ also undergoes a positional shift, which seems to be approximately constant in the range of $0.5 \leq x \leq 0.9$ and which is mainly along the b axis. The structural distortion of $X2$ increases for $x < 0.5$, which then is mainly a shift along a and c. The A site cation remains almost on the pseudo-cubic position for $0.5 \leq x \leq 0.9$ and moves away from that point for $x < 0.5$, but the total shift is lower by almost an order of magnitude compared to $X1/X2$. The shift of the A cation can be determined by an increasing intensity of some superstructure reflections in the XRD pattern, which is very indicative for the (2 1 0) peak. This reflection also allows for an assignment of the a and c axes, since the (0 1 2) reflection is extinguished ($0\,k\,l$: $k+l=2n$) in the space group $Pnma$. By this shift, A is further lowering its ECoN from 8.5 for $La_{0.5}Sr_{0.5}FeO_{2.5}F_{0.5}$ to 7.3 for $La_{0.9}Sr_{0.1}FeO_{2.9}F_{0.1}$ (see also Fig. 8), but to a smaller extent than by the shift of $X1$. All things considered, the lattice parameter behavior can be explained by a sort of two-step structural relaxation process on La doping: for increasing La content (decreasing x), the movements of La and $X2$ in the range $0.5 \geq x \geq 0$ decrease the former deviation of $(a,b,c)_{norm}$ from 1, which was caused by the shift of $X1$ in the range $1 \geq x \geq 0.5$. A pictorial of these effects is given in Fig. 9, which also illustrates the tilting of the octahedra.

4. Conclusions

Samples of composition $La_{1-x}Sr_xFeO_{3-\delta}$ were prepared via a high temperature solid state route. For decreasing x, several structural changes can be observed going from tetragonal ($I4/mmm$, $x=1.0$-0.9), to cubic (Pm-$3m$, $x=0.8$-0.7), to rhombohedral (R-$3c$, $x=0.6$-0.5) and to orthorhombic ($Pnma$, $x=0.1$-0.0). For $0.2 \leq x \leq 0.4$, two phase mixtures of the rhombohedral and the orthorhombic phases were obtained. Furthermore, we showed that the degree of metric distortion from cubic symmetry is biggest for compositions in the range $0.2 \leq x \leq 0.5$.

The kinetically stabilized phases $La_{1-x}Sr_xFeO_{3-x}F_x$ can be prepared via low temperature fluorination of the precursor oxides using PVDF. The oxyfluorides crystallize in an orthorhombic distorted perovskite structure ($Pnma$, $0.1 \leq x \leq 0.9$) and are isotypic to $LaFeO_3$. $SrFeO_2F$ is found as a cubic perovskite (Pm-$3m$). The metric distortion from cubic symmetry $(a,b,c)_{norm}$ reveals a two-step structural relaxation for decreasing x, where $X1$ shifts from its position in a cubic setting for $0.1 \leq x \leq 0.9$, and $X2$ and A only show a remarkable shift for $0.1 \leq x \leq 0.5$ in the direction of a and c. The structural distortion is found to be accompanied by the lowering of the coordination needs of the A site cation. Additionally, we showed that the oxyfluorides are not stable and decompose at higher temperatures, where quantification of the decomposition products can be utilized to confirm the oxyfluoride composition for Sr rich samples.

References

[1] J. Mizusaki, M. Yoshihiro, S. Yamauchi, K. Fueki, J. Solid State Chem. 58 (1985) 257–266.
[2] G. Deng, Y. Chen, M. Tao, C. Wu, X. Shen, H. Yang, Electrochim. Acta 54 (2009) 3910–3914.
[3] D. Bayraktar, S. Diethelm, T. Graule, J. Van herle, P. Holtappels, J. Electroceram. 22 (2009) 55-60-60.
[4] H.J. Wei, Y. Cao, W.J. Ji, C.T. Au, Catal. Commun. 9 (2008) 2509–2514.
[5] L. Nalbandian, A. Evdou, V. Zaspalis, Int. J. Hydrogen Energy 34 (2009) 7162–7172.
[6] P.A. Murade, V.S. Sangawar, G.N. Chaudhari, V.D. Kapse, A.U. Bajpeyee, Curr. Appl. Phys. 11 (2011) 451–456.
[7] M. Kuhn, S. Hashimoto, K. Sato, K. Yashiro, J. Mizusaki, Solid State Ionics 195 (2011) 7–15.
[8] J. Mizusaki, T. Sasamoto, W.R. Cannon, H.K. Bowen, J. Am. Ceram. Soc. 66 (1983) 247–252.
[9] M. Søgaard, P. Vang Hendriksen, M. Mogensen, J. Solid State Chem. 180 (2007) 1489–1503.
[10] J.S. Waugh, Technical Report No. 152, Laboratory for Insulation Research, Massachusetts Institute of Technology, 1960.
[11] S.E. Dann, D.B. Currie, M.T. Weller, M.F. Thomas, A.D. Al-Rawwas, J. Solid State Chem. 109 (1994) 134–144.
[12] M. Takano, J. Kawachi, N. Nakanishi, Y. Takeda, J. Solid State Chem. 39 (1981) 75–84.
[13] P.R. Slater, P.P. Edwards, C. Greaves, I. Gameson, M.G. Francesconi, J.P. Hodges, M. Al-Mamouri, M. Slaski, Physica C (Amsterdam, Neth.) 241 (1995) 151–157.
[14] P.R. Slater, J.P. Hodges, M.G. Francesconi, P.P. Edwards, C. Greaves, I. Gameson, M. Slaski, Physica C (Amsterdam, Neth.) 253 (1995) 16–22.
[15] E.I. Ar-nikova, S.V. Lubarsky, D.I. Denisenko, R.V. Shpanchenko, E.V. Antipov, G. Van Tendeloo, Physica C (Amsterdam, Neth.) 253 (1995) 259–265.
[16] P.R. Slater, J. Fluorine Chem. 117 (2002) 43–45.
[17] I.O. Troyanchuk, N.V. Kasper, O.S. Mantytskaya, E.F. Shapovalova, Mater. Res. Bull. 30 (1995) 421–425.
[18] P.R. Slater, R.K.B. Gover, J. Mater. Chem. 12 (2002) 291–294.
[19] P.R. Slater, J.P. Hodges, M.G. Francesconi, C. Greaves, M. Slaski, J. Mater. Chem. 7 (1997) 2077–2083.
[20] F.J. Berry, X. Ren, R. Heap, P. Slater, M.F. Thomas, Solid State Commun. 134 (2005) 621–624.
[21] R. Heap, P.R. Slater, F.J. Berry, O. Helgason, A.J. Wright, Solid State Commun. 141 (2007) 467–470.
[22] O. Clemens, R. Haberkorn, P.R. Slater, H.P. Beck, Solid State Sci. 12 (2010) 1455–1463.
[23] Ö. Helgason, Hyperfine Interact. 184 (2008) 143–146.
[24] F.J. Berry, A.F. Bowfield, F.C. Coomer, S.D. Jackson, E.A. Moore, P.R. Slater, M.F. Thomas, A.J. Wright, X. Ren, J. Phys.: Condens. Matter 21 (2009) 256001.
[25] F.J. Berry, X. Ren, R. Heap, P. Slater, M.F. Thomas, J. Phys. Chem. Solids 69 (2008) 2032–2036.
[26] F.J. Berry, et al., J. Phys.: Condens. Matter 20 (2008) 215207.
[27] F.J. Berry, F.C. Coomer, C. Hancock, Ö. Helgason, E.A. Moore, P.R. Slater, A.J. Wright, M.F. Thomas, J. Solid State Chem. 184 (2011) 1361–1366.
[28] M. Sturza, S. Daviero-Minaud, H. Kabbour, O. Gardoll, O. Mentré, Chem. Mater. 22 (2010) 6726–6735.
[29] Topas V4.2, General profile and structure analysis software for powder diffraction data, User's Manual. Bruker AXS, Karlsruhe, 2008.

[30] R.W. Cheary, A.A. Coelho, J.P. Cline, J. Res. Nat. Inst. Stand. Technol. 109 (2004) 1–25.

[31] J. Blasco, J. Stankiewicz, J. García, J. Solid State Chem. 179 (2006) 898–908.

[32] J.P. Hodges, S. Short, J.D. Jorgensen, X. Xiong, B. Dabrowski, S.M. Mini, C.W. Kimball, J. Solid State Chem. 151 (2000) 190–209.

[33] E.G. Ippolitov, L.S. Garashina, A.G. Maklachkov, Inorg. Mater. 3 (1967) 59–62.

[34] M. Sturza, H. Kabbour, S. Daviero-Minaud, D. Filimonov, K. Pokholok, N. Tiercelin, F. Porcher, L. Aldon, O. Mentre, J. Am. Chem. Soc. 133 (2011) 10901–10909.

[35] R.D. Shannon, Acta Crystallogr. A32 (1976) 751–767.

[36] Y. Takeda, K. Kanno, T. Takada, O. Yamamoto, M. Takano, N. Nakayama, Y. Bando, J. Solid State Chem. 63 (1986) 237–249.

[37] F. Deganello, L.F. Liotta, A. Longo, M.P. Casaletto, M. Scopelliti, J. Solid State Chem. 179 (2006) 3406–3419.

[38] U. Müller, Anorganische Strukturchemie, B. G. Teubner Verlag, Wiesbaden, 2004.

[39] R. Hoppe, Z. Kristallogr. 150 (1979) 23–52.